

文章编号: 1001-3555(2021)03-0263-10

## 硫化镍和磷化镍的 HDS 加氢活性和稳定性

袁亚梅, 陈 慧\*, 赵丹阳, 吴 驰, 耿 皎\*, 沈俭一\*

(南京大学 化学化工学院 介观化学教育部重点实验室, 江苏 南京 210023)

**摘要:** 采用共沉淀法制备了高分散 80%Ni/Al<sub>2</sub>O<sub>3</sub> 催化剂, 经 350 °C 焙烧, 得高分散 NiO/Al<sub>2</sub>O<sub>3</sub> (NiO 粒径 ~3 nm), 将其以 CS<sub>2</sub> 硫化(310 °C, 4 h) 或 PPh<sub>3</sub> 磷化(320 °C, 36 h), 分别获得了高分散的硫化镍(Ni<sub>3</sub>S<sub>2</sub> 和 Ni<sub>3</sub>S<sub>4</sub>, 5.8 nm) 和 Ni<sub>2</sub>P(7.0 nm), 在二苯并噻吩(DBT)的加氢脱硫(HDS)反应中, Ni<sub>2</sub>P 的活性远高于 NiS<sub>x</sub> (360 °C 时 DBT 的转化率分别为 100% 和 75%)。若将 NiS<sub>x</sub> 用 PPh<sub>3</sub> 磷化, 则 NiS<sub>x</sub> 全部转化为 Ni<sub>2</sub>P(13.3 nm), 其 HDS 活性远高于原来的 NiS<sub>x</sub> 且与直接磷化获得的 Ni<sub>2</sub>P(7.0 nm) 相当。反之, 若将 Ni<sub>2</sub>P 用 CS<sub>2</sub> 硫化, 则 Ni<sub>2</sub>P 物相不变, 粒径也没有长大, 表明 Ni<sub>2</sub>P 物相远比 NiS<sub>x</sub> 稳定, 且其 HDS 活性高于直接磷化的 Ni<sub>2</sub>P, 表明其 Ni<sub>2</sub>P 表面可能生成了 HDS 活性更高的某种 Ni-P-S 物种。

**关键词:** Ni<sub>2</sub>P/Al<sub>2</sub>O<sub>3</sub> 催化剂; NiS<sub>x</sub>/Al<sub>2</sub>O<sub>3</sub> 催化剂; PPh<sub>3</sub> 液相磷化; CS<sub>2</sub> 液相硫化; 物相稳定性; 加氢精制反应

**中图分类号:** O643.3

**文献标志码:** A

**DOI:** 10.16084/j.issn1001-3555.2021.03.007

硫化镍本身在加氢精制反应中的加氢脱硫(HDS)活性并不理想, 主要作为硫化钼或钨体系的助催化剂, 组成  $\gamma$ -Al<sub>2</sub>O<sub>3</sub> 或 SiO<sub>2</sub> 负载的 Ni-Mo-S 和 Ni-W-S 催化剂。磷化镍具有较高的 HDS、加氢脱氮(HDN)活性和较高的耐硫性能, 有可能替代传统的过渡金属硫化物催化剂用于加氢精制反应。文献中关于硫化镍和磷化镍的比较研究很少。由于原料和制备方法对催化剂的组成和性能影响很大, 比较硫化镍和磷化镍并非易事。

我们采用共沉淀法制备了高担载量和高分散度的 80%Ni/Al<sub>2</sub>O<sub>3</sub> 催化剂, 经 350 °C 焙烧后获得了高分散的 NiO/Al<sub>2</sub>O<sub>3</sub> 催化剂前驱体, 其中 NiO 的粒径约为 3 nm。用 CS<sub>2</sub> 在 310 °C 将 NiO/Al<sub>2</sub>O<sub>3</sub> 硫化 4 h, 获得了高分散的硫化镍(Ni<sub>3</sub>S<sub>2</sub> 和 Ni<sub>3</sub>S<sub>4</sub>), 粒径约为 5.8 nm。用三苯基膦(PPh<sub>3</sub>)将上述硫化镍磷化, 如果磷化温度较低(170~220 °C), 硫化镍就无法被磷化, 但其粒径会逐渐增大至 8.4 nm。在 270 °C 时部分硫化镍已被磷化成 Ni<sub>2</sub>P, 粒径增大至 11.7 nm。磷化温度升至 320 °C, 硫化镍全部转化为 Ni<sub>2</sub>P, 得到 NiS<sub>x</sub>(P)/Al<sub>2</sub>O<sub>3</sub> 催化剂, Ni<sub>2</sub>P 粒径也进一步增大到 13.3 nm。

如果将所得的 Ni/Al<sub>2</sub>O<sub>3</sub> 用 PPh<sub>3</sub> 在 320 °C 磷化 36 h, NiO 就转化为纯 Ni<sub>2</sub>P 物相(粒径约为 7.0 nm),

得到 Ni<sub>2</sub>P/Al<sub>2</sub>O<sub>3</sub> 催化剂。用 CS<sub>2</sub> 硫化 Ni<sub>2</sub>P/Al<sub>2</sub>O<sub>3</sub> 时, 即使温度提高到 360 °C, 催化剂中仍只检测到 Ni<sub>2</sub>P 物相, 表明 Ni<sub>2</sub>P 物相比硫化镍(Ni<sub>3</sub>S<sub>2</sub> 和 Ni<sub>3</sub>S<sub>4</sub>)物相更加稳定, 难以被 CS<sub>2</sub> 硫化, 这是 Ni<sub>2</sub>P 具有较高耐硫性能的重要原因。硫化后的 Ni<sub>2</sub>P(S)/Al<sub>2</sub>O<sub>3</sub> 催化剂中 Ni<sub>2</sub>P 粒径增大到 9.5 nm, 但仍比 320 °C 磷化硫化镍得到的 Ni<sub>2</sub>P 的粒径(13.3 nm)小得多, 证明 Ni<sub>2</sub>P 物相和粒径都比较稳定。

分析催化剂的化学组成发现, 硫化镍经 PPh<sub>3</sub> 磷化后仅剩余了 3% 的 S, 即绝大部分 S 已被 P 取代, NiS<sub>x</sub> 转化成了 Ni<sub>2</sub>P, 而磷化镍经 CS<sub>2</sub> 硫化后只有 1.1% 的 S 进入催化剂中, 且未检测到硫化物物相, 表明 Ni<sub>2</sub>P 确实具有很强的抗硫性能。此外, 无论是将硫化镍磷化, 还是将磷化镍硫化, 所得样品中 P/Ni 比值相似(0.74), 均高于 Ni<sub>2</sub>P 的化学计量比 0.5, 说明除了 Ni<sub>2</sub>P 外, 催化剂中还可能还存在富磷磷化镍或其他含 P 物种。

将上述直接磷化或硫化得到的 Ni<sub>2</sub>P/Al<sub>2</sub>O<sub>3</sub> 和 NiS<sub>x</sub>/Al<sub>2</sub>O<sub>3</sub> 催化剂, 以及硫化镍再磷化(NiS<sub>x</sub>(P)/Al<sub>2</sub>O<sub>3</sub>)和磷化镍再硫化(Ni<sub>2</sub>P(S)/Al<sub>2</sub>O<sub>3</sub>)后的催化剂分别用于模型柴油(含 1.72% (质量分数)的二苯并噻吩(DBT)、0.185% (质量分数)的喹啉、5% (质量分数)的四氢萘)的加氢精制反应。反应后, Ni<sub>2</sub>P/

收稿日期: 2020-11-08; 修回日期: 2021-01-13.

**基金项目:** 本工作受到国家自然科学基金面上项目(21773108)、国家自然科学基金中德合作项目(21761132006)和中央高校基本科研业务费资助(This work was financially supported by the NSFC(21773108), NSFC-DFG(21761132006) and fundamental research funds for central universities).

**作者简介:** 袁亚梅, 女, 1989 年生, 博士(YUAN Yamei, female, born in 1989, PhD).

\* 通讯联系人, E-mail: jyshen@nju.edu.cn; Tel: 025-89684305.

$\text{Al}_2\text{O}_3$  和  $\text{NiS}_x/\text{Al}_2\text{O}_3$  催化剂的物相都没有发生变化, 表明  $\text{Ni}_2\text{P}$  和  $\text{NiS}_x$  物相在加氢精制反应过程中均是稳定的.  $\text{NiS}_x(\text{P})/\text{Al}_2\text{O}_3$  经过 HDS 反应,  $\text{Ni}_2\text{P}$  的 XRD 衍射峰依然存在, 且较强, 表明该催化剂在反应条件下没有被 DBT 硫化, 即由硫化镍磷化而转化来的  $\text{Ni}_2\text{P}$  在加氢精制反应条件下也是稳定的.  $\text{Ni}_2\text{P}(\text{S})/\text{Al}_2\text{O}_3$  经过 HDS 反应, 仍以  $\text{Ni}_2\text{P}$  物相为主, 但出现了  $\text{NiP}_2$ , 可能是因为催化剂中残留了过量 P, 它在温度较高时与  $\text{Ni}_2\text{P}$  反应, 生成了过磷化物  $\text{NiP}_2$ .

在 DBT 的 HDS 反应中,  $\text{Ni}_2\text{P}/\text{Al}_2\text{O}_3$  的 HDS 活性远高于  $\text{NiS}_x/\text{Al}_2\text{O}_3$ . 在 360 °C 时, 以  $\text{Ni}_2\text{P}$  为主要物相的  $\text{Ni}_2\text{P}/\text{Al}_2\text{O}_3$ 、 $\text{NiS}_x(\text{P})/\text{Al}_2\text{O}_3$  和  $\text{Ni}_2\text{P}(\text{S})/\text{Al}_2\text{O}_3$  的 DBT 加氢脱硫活性均达到了 100%, 而  $\text{NiS}_x/\text{Al}_2\text{O}_3$  的 DBT 转化率只有 75%. 同时,  $\text{Ni}_2\text{P}(\text{S})/\text{Al}_2\text{O}_3$  的 HDS 活性高于  $\text{Ni}_2\text{P}/\text{Al}_2\text{O}_3$ , 例如在 260 °C 时, 它们的 HDS 转化率分别为 66% 和 45%.  $\text{Ni}_2\text{P}$  在  $\text{CS}_2$  硫化时物相没有发生变化, 但有 1.1% 的 S 进入了催化剂, 表明  $\text{Ni}_2\text{P}$  经  $\text{CS}_2$  硫化后有 Ni-P-S 表面物种生成, 其 HDS 加氢活性高于纯  $\text{Ni}_2\text{P}$ .  $\text{NiS}_x(\text{P})/\text{Al}_2\text{O}_3$  中也含有 3% 的 S, 但其 HDS 活性却与  $\text{Ni}_2\text{P}/\text{Al}_2\text{O}_3$  差别不大, 可能是由于  $\text{NiS}_x(\text{P})/\text{Al}_2\text{O}_3$  中  $\text{Ni}_2\text{P}$  的粒径(13.0 nm)远大于  $\text{Ni}_2\text{P}/\text{Al}_2\text{O}_3$  的粒径(7.0 nm). 可见, 由于 S 的存在,  $\text{NiS}_x(\text{P})/\text{Al}_2\text{O}_3$  中  $\text{Ni}_2\text{P}$  的活性还是显著提高了. 因此, 在 360 °C, DBT 在这些催化剂上的转化率顺序为:  $\text{Ni}_2\text{P}(\text{S})/\text{Al}_2\text{O}_3 > \text{NiS}_x(\text{P})/\text{Al}_2\text{O}_3 > \text{Ni}_2\text{P}/\text{Al}_2\text{O}_3 \gg \text{NiS}_x/\text{Al}_2\text{O}_3$ .

在产物选择性方面, 随着反应温度提高, 所有催化剂上生成环己基苯(CHB)的选择性增大, 表明在这些催化剂上, DBT 的 HDS 反应以先加氢再脱硫路线为主, 而非生成联苯(BP)产物的直接脱硫路线. 4 个催化剂上 HDS 反应生成 CHB 的选择性顺序为  $\text{Ni}_2\text{P}/\text{Al}_2\text{O}_3 > \text{NiS}_x(\text{P})/\text{Al}_2\text{O}_3 > \text{Ni}_2\text{P}(\text{S})/\text{Al}_2\text{O}_3 > \text{NiS}_x/\text{Al}_2\text{O}_3$ , 表明催化剂中的 S 不利于加氢脱硫反应路线.

在 260~360 °C 下, 4 种催化剂都表现出很高的加氢脱氮活性, 喹啉转化率均达到 100%. 虽然各催化剂上丙基环己烷(PCH)的选择性都随反应温度提高而提高, 但不同催化剂对 PCH 的选择性也存在差异(较低温度下尤为明显). 260 °C 时,  $\text{NiS}_x/\text{Al}_2\text{O}_3$ 、 $\text{Ni}_2\text{P}/\text{Al}_2\text{O}_3$ 、 $\text{Ni}_2\text{P}(\text{S})/\text{Al}_2\text{O}_3$  和  $\text{NiS}_x(\text{P})/\text{Al}_2\text{O}_3$  上的 PCH 选择性依次为 30%、90%、80% 和 88%. 可见,  $\text{Ni}_2\text{P}$  对喹啉的苯环加氢活性远高于硫化镍.

不同方法得到的磷化镍对四氢萘加氢精制反应

的催化活性均远高于硫化镍. 例如, 360 °C 时四氢萘在  $\text{NiS}_x/\text{Al}_2\text{O}_3$  上的转化率仅有 0.6%, 但在  $\text{NiS}_x(\text{P})/\text{Al}_2\text{O}_3$ 、 $\text{Ni}_2\text{P}/\text{Al}_2\text{O}_3$  和  $\text{Ni}_2\text{P}(\text{S})/\text{Al}_2\text{O}_3$  上四氢萘的转化率分别达到了 5.7%、9.2% 和 13.8%, 与催化剂的 DBT 加氢脱硫活性顺序一致. 四氢萘在加氢精制反应中既可发生加氢反应生成反式和顺式十氢萘, 也可发生脱氢反应生成萘.  $\text{Ni}_2\text{P}$  的十氢萘选择性远高于  $\text{NiS}_x$ , 而含硫  $\text{Ni}_2\text{P}$  催化剂的十氢萘选择性则降低了, 再次表明  $\text{Ni}_2\text{P}$  中含硫不利于芳环加氢反应.

## 1 Introduction

Nickel sulfides have various applications in the fields such as semiconductors, optoelectronics, energy and catalysis<sup>[1-5]</sup>. However, they are not highly active for the hydrotreating reactions<sup>[6-10]</sup>, and were mainly used as promoters for the supported Ni-Mo-S and Ni-W-S catalysts<sup>[11-13]</sup>. On the other hand, the transition metal phosphides (especially  $\text{Ni}_2\text{P}$ ) were found to be highly active for the hydrotreating reactions and expected to become a new generation of catalysts to play the same functions as the traditional catalysts of metal sulfides. In fact, different techniques have been developed for the preparation of metal phosphides, for example, the technique of temperature-programmed reduction (TPR), the gas phase phosphidation with  $\text{PH}_3$  and liquid phase phosphidation with  $\text{PPh}_3$ <sup>[14-16]</sup>.

Only a few comparative studies on the nickel sulfides and phosphides were reported in literature. Phimsen *et al.*<sup>[17]</sup> prepared a 15%Ni/ $\text{Al}_2\text{O}_3$  catalyst, which was sulfided by  $\text{H}_2\text{S}/\text{H}_2$  to nickel sulfides ( $\text{Ni}_3\text{S}_2$  and  $\text{Ni}_3\text{S}_4$ ) or phosphided by the TPR method to nickel phosphides ( $\text{Ni}_{12}\text{P}_5$  and  $\text{Ni}_3\text{P}$ ). They found that the nickel phosphides showed the higher hydrogenation and hydrodeoxygenation activities than the nickel sulfides while the nickel sulfides exhibited the lower methanation and cracking activities than the nickel phosphides for the production of bio-fuels from the spent coffee oil. Stinner *et al.*<sup>[18]</sup> found that the presence of  $\text{H}_2\text{S}$  in feed strongly inhibited the hydrodenitridation (HDN) activity of a  $\text{Ni}_2\text{P}$  catalyst, and the activity could not be recovered even after the removal of  $\text{H}_2\text{S}$  from the feed. The authors argued that  $\text{Ni}_2\text{P}$  was more stable than  $\text{NiS}_x$  and  $\text{Ni}_2\text{P}$  could not be sulfided by

H<sub>2</sub>S so that the decrease of HDN activity must be due to the irreversible block of active sites of Ni<sub>2</sub>P by the strongly adsorbed H<sub>2</sub>S. However, others reported that sulfur could be incorporated into the surface of metal phosphides during the HDS reactions. For example, Oyama *et al.* [19–20] detected Ni-S bonds on the surface of used nickel phosphides, suggesting the formation of nickel phosphosulfide surface species, which might be the real active species for the HDS reactions. Wang *et al.* [21] found that the Ni<sub>2</sub>P/MCM-41 passivated by H<sub>2</sub>S was more active than that passivated by O<sub>2</sub> for the HDS reaction, and the catalyst with the higher HDS activity contained more sulfur after the reaction. The authors also suggested that the surface sulfides or phosphosulfide species were the active sites for the HDS reaction. Similar results were obtained on the FeP/SiO<sub>2</sub> prepared with FeS as the precursor [22]. Nelson *et al.* [23] indicated that up to 50% of surface P atoms in Ni<sub>2</sub>P could be replaced by S according to their DFT calculations.

It is not easy to adequately compare nickel sulfides with phosphides since different precursors and preparation methods could significantly affect the composition and performance of catalysts. To a large extent, the relatively low HDS activities of nickel sulfides might be due to their low surface area, poor dispersion and thus little active sites [7–9]. It can be expected that more active sites and consequently higher HDS activity could be achieved with nickel sulfides. Recently, highly dispersed Ni<sub>2</sub>P [16,24–27] and Fe<sub>2</sub>P [28–29] catalysts were prepared in our group, with the highly loaded (60%~80% weight percent) and dispersed precursors. The Ni<sub>2</sub>P catalysts thus prepared possessed small particles and abundant active sites and exhibited high activities for the HDS reactions of dibenzothiophene (DBT). In particular, the phosphidation of the 80% Ni/Al<sub>2</sub>O<sub>3</sub> (with the high H<sub>2</sub> uptake of 1017 μmol/g) generated a Ni<sub>2</sub>P/Al<sub>2</sub>O<sub>3</sub> catalyst with the CO uptake of 345 μmol/g, which is the highest value reported so far [26]. In this work, the similar nickel precursor was used to prepare nickel sulfides and compared with Ni<sub>2</sub>P. However, since the nickel sulfides were prepared by the direct sulfidation

with CS<sub>2</sub>, Ni<sub>2</sub>P in comparison must be prepared via the direct phosphidation with the same calcined precursor without the pre-reduction. In brief, the highly dispersed 80% Ni/Al<sub>2</sub>O<sub>3</sub> catalyst was prepared, calcined and then sulfided by CS<sub>2</sub> or phosphided by PPh<sub>3</sub> in liquid phases to obtain the highly dispersed nickel sulfides (NiS<sub>x</sub>) or Ni<sub>2</sub>P catalysts. Then the NiS<sub>x</sub> (or Ni<sub>2</sub>P) was further treated by PPh<sub>3</sub> (or CS<sub>2</sub>) to observe the phase changes. All the catalysts were tested for the HDS of DBT, HDN of quinoline and hydrogenation of tetralin.

## 2 Experimental

### 2.1 Preparation of catalysts

The Ni/Al<sub>2</sub>O<sub>3</sub> with about 80% Ni in weight was prepared by the co-precipitation method and dried with *n*-butanol [26]. In brief, desired amounts of Ni (NO<sub>3</sub>)<sub>2</sub> and Al (NO<sub>3</sub>)<sub>3</sub> were dissolved in 100 mL de-ionized water to obtain a solution, while desired amount of Na<sub>2</sub>CO<sub>3</sub> was dissolved in 100 mL de-ionized water to obtain another solution. The two solutions were simultaneously added drop-wise into 200 mL de-ionized water under stirring at 80 °C. The precipitate formed was washed thoroughly with de-ionized water, and then dispersed into 200 mL *n*-butanol which was evaporated at 80 °C. The sample was then further dried at 120 °C for 12 h, and calcined in air at 350 °C for 3 h. The sample thus obtained was denoted as NiO/Al<sub>2</sub>O<sub>3</sub>.

The sample was sulfided by CS<sub>2</sub> in liquid phase [29–30]. Typically, the NiO/Al<sub>2</sub>O<sub>3</sub> was loaded into a fix-bed reactor with an inner diameter of 10 mm and sandwiched with quartz sands. Then, a heptanes solution containing 2% (weight percentage) CS<sub>2</sub> was pumped into the reactor along with H<sub>2</sub> flow at a weight hourly space velocity (WHSV) of 2 h<sup>-1</sup> and H<sub>2</sub>/oil of 300 v/v. The reactor was heated from room temperature to 230 °C with a rate of 1 °C/min, kept at 230 °C for 2 h, then heated to 310 °C with the same rate, and kept at 310 °C for 4 h. The sample thus sulfided directly was denoted as NiS<sub>x</sub>/Al<sub>2</sub>O<sub>3</sub>.

The NiO/Al<sub>2</sub>O<sub>3</sub> was phosphided by PPh<sub>3</sub> in liquid phase [26]. The procedure was similar to that of sulfidation above, but a heptane solution containing 2% (weight percentage) PPh<sub>3</sub> was used here. The

temperature was elevated to 320 °C with the rate of 1 °C/min and kept at 320 °C for 36 h. The catalyst thus phosphidized directly was denoted as  $\text{Ni}_2\text{P}/\text{Al}_2\text{O}_3$ .

Then, the  $\text{NiS}_x/\text{Al}_2\text{O}_3$  was treated by  $\text{PPh}_3$  with the same phosphidation procedure described above and the sample obtained was denoted as  $\text{NiS}_x(\text{P})/\text{Al}_2\text{O}_3$ . Similarly, the  $\text{Ni}_2\text{P}/\text{Al}_2\text{O}_3$  was treated by  $\text{CS}_2$  with the same sulfidation procedure described above and the sample obtained was denoted as  $\text{Ni}_2\text{P}(\text{S})/\text{Al}_2\text{O}_3$ .

## 2.2 Characterization of catalysts

The catalysts for characterizations were passivated before unloaded from the fix-bed reactor. X-ray diffraction (XRD) patterns were collected on a Shimadzu XRD-6000 powder diffractometer using a  $\text{Cu } K\alpha$  radiation ( $\lambda = 0.1541 \text{ nm}$ ) at 40 kV and 30 mA. The  $2\theta$  scans covered the range of  $10^\circ$  to  $80^\circ$  with a speed of  $6 (^\circ)/\text{min}$  and a step of  $0.02^\circ$ . The chemical compositions of catalysts were analyzed by an ARL-9800 X-ray fluorescence spectrometer (XRF).

## 2.3 Catalytic tests

Model diesel containing 1.72% DBT, 0.185% quinoline, 5% tetralin and 0.5% n-octane (as an internal standard) in balanced n-tetradecane (solvent) was pumped into a tubular stainless steel fix-bed reactor with an inner diameter of 10 mm for the evaluation of catalysts at 260~360 °C, 3.1 MPa with a WHSV of  $2 \text{ h}^{-1}$  and  $\text{H}_2/\text{oil}$  ratio of 1500 (v/v). The products were collected after 24 h when the activity was stabilized, and analyzed on a gas chromatograph equipped with a flame ionization detector (FID), a flame photometric detector (FPD) and a nitrogen-phosphorus detector (NPD).

# 3 Results and discussion

## 3.1 Phosphidation of $\text{NiS}_x$

Fig.1 shows the XRD patterns for the  $\text{NiO}/\text{Al}_2\text{O}_3$ ,  $\text{NiS}_x/\text{Al}_2\text{O}_3$  and the samples derived from the phosphidations of  $\text{NiS}_x/\text{Al}_2\text{O}_3$  at 170~320 °C for 36 h, respectively. Only broad diffraction peaks for NiO (PDF 65-2901) were detected for the calcined sample (Fig.1 (a)), indicating that small NiO particles (about 3 nm) were highly dispersed on the support. When the  $\text{NiO}/\text{Al}_2\text{O}_3$  was sulfided by  $\text{CS}_2$  at 310 °C, the diffraction peaks

for NiO disappeared, and new peaks for  $\text{Ni}_3\text{S}_2$  (PDF 44-1418) appeared at  $2\theta = 21.7^\circ$ ,  $31.1^\circ$ ,  $37.7^\circ$ ,  $44.3^\circ$ ,  $49.7^\circ$  and  $55.2^\circ$  and those for  $\text{Ni}_3\text{S}_4$  (PDF 43-1469) appeared at  $2\theta = 26.5^\circ$ ,  $31.3^\circ$ ,  $37.9^\circ$ ,  $49.9^\circ$  and  $54.8^\circ$  (Fig.1 (b)), indicating the formation of nickel sulfides (denoted as  $\text{NiS}_x$ ) upon the direct sulfidation of  $\text{NiO}/\text{Al}_2\text{O}_3$  by  $\text{CS}_2$ .

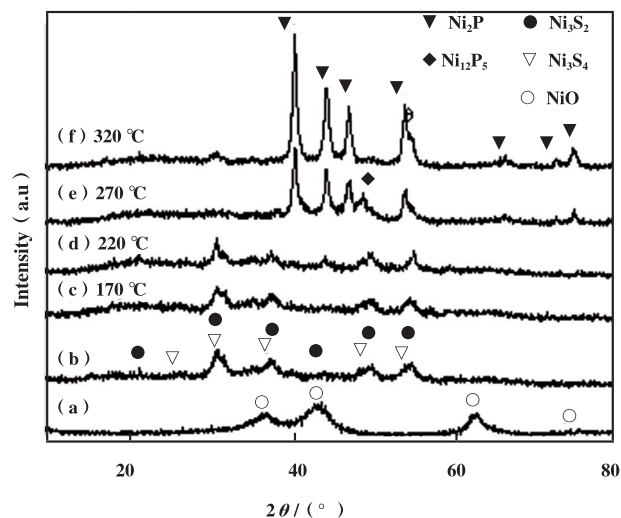


Fig.1 XRD patterns for the  $\text{Ni}/\text{Al}_2\text{O}_3$  calcined at 350 °C (a), followed by sulfidation of (a) at 310 °C for 4 h (b) and then phosphidation of (b) at 170~320 °C for 36 h (c-f), respectively

Fig.1 (c-f) show the XRD patterns for the  $\text{NiS}_x/\text{Al}_2\text{O}_3$  phosphidated at different temperatures (170~320 °C) for 36 h. When the  $\text{NiS}_x/\text{Al}_2\text{O}_3$  was phosphidated at 170 and 220 °C, only  $\text{Ni}_3\text{S}_2$  and  $\text{Ni}_3\text{S}_4$  phases were observed (Fig.1 (c) and (d)), indicating that  $\text{NiS}_x$  could not be phosphidated at the low temperatures. However, the intensities of diffraction peaks for  $\text{NiS}_x$  increased, indicating the increase in the crystalline sizes of  $\text{NiS}_x$  during the phosphidation. When the  $\text{NiS}_x/\text{Al}_2\text{O}_3$  was phosphidated at 270 °C, the diffraction peaks for  $\text{NiS}_x$  disappeared, and the diffraction peaks for  $\text{Ni}_2\text{P}$  (PDF 65-1989) appeared at  $2\theta = 40.7^\circ$ ,  $44.6^\circ$ ,  $47.4^\circ$  and  $54.2^\circ$  and those for  $\text{Ni}_{12}\text{P}_5$  (PDF 22-1190) appeared at  $2\theta = 48.9^\circ$  (Fig.1 (e)), indicating the replacement of S in  $\text{NiS}_x$  by P during the process. When the phosphidation temperature increased to 320 °C, the diffraction peak for  $\text{Ni}_{12}\text{P}_5$  disappeared while the intensities of peaks for  $\text{Ni}_2\text{P}$  increased significantly (Fig.1 (f)),



indicating the complete conversion of  $\text{NiS}_x$  to  $\text{Ni}_2\text{P}$  ( $\text{NiS}_x(\text{P})/\text{Al}_2\text{O}_3$ ) and growing of the  $\text{Ni}_2\text{P}$  particles.

Table 1 summarizes the information of the phases and crystalline sizes for the samples (a–f) in Fig.1. The crystalline size of NiO obtained by the calcination of Ni/ $\text{Al}_2\text{O}_3$  at 350 °C was estimated to be about 3 nm, while the direct sulfidation led to the formation of  $\text{NiS}_x$  with the average crystalline size of about 5.8 nm. Although the  $\text{NiS}_x$  was not phosphided by  $\text{PPh}_3$  at the lower temperatures, the crystalline sizes of  $\text{NiS}_x$  were gradually increased to 8.4 nm. When  $\text{NiS}_x$  was phosphided at 320 °C, the crystalline size of formed  $\text{Ni}_2\text{P}$  grew larger to about 13.3 nm.

Table 1 Phases and crystalline sizes in the catalysts prepared by different methods

Samples in Fig.1	XRD phase	D /nm
a	NiO	3.0
b	$\text{Ni}_3\text{S}_2$ , $\text{Ni}_3\text{S}_4$	5.8
c	$\text{Ni}_3\text{S}_2$ , $\text{Ni}_3\text{S}_4$	5.8
d	$\text{Ni}_3\text{S}_2$ , $\text{Ni}_3\text{S}_4$	8.4
e	$\text{Ni}_2\text{P}/\text{Ni}_{12}\text{P}_5$	11.7/8.2
f	$\text{Ni}_2\text{P}$	13.3

Notes: The crystalline sizes (D) were estimated by the Scherrer equation according to the full width at half maximum (FWHM) of the peaks at 43.2° (NiO), 40.8° ( $\text{Ni}_2\text{P}$ ), 48.9° ( $\text{Ni}_{12}\text{P}_5$ ) and 31.1° ( $\text{Ni}_3\text{S}_2$ ), respectively, in the XRD patterns.

### 3.2 Sulfidation of $\text{Ni}_2\text{P}$

Fig.2 shows the XRD patterns for the  $\text{NiO}/\text{Al}_2\text{O}_3$ ,  $\text{Ni}_2\text{P}/\text{Al}_2\text{O}_3$  and those obtained by the sulfidation of  $\text{Ni}_2\text{P}/\text{Al}_2\text{O}_3$  at 310~360 °C, respectively. When the  $\text{NiO}/\text{Al}_2\text{O}_3$  was phosphided by  $\text{PPh}_3$  at 320 °C, pure  $\text{Ni}_2\text{P}$  phase was obtained (Fig.2 (b)). However, when the  $\text{Ni}_2\text{P}/\text{Al}_2\text{O}_3$  was treated by  $\text{CS}_2$  at even higher temperature (360 °C), the  $\text{Ni}_2\text{P}$  was still the only phase detected by XRD, indicating that the  $\text{Ni}_2\text{P}$  was significantly more stable than the sulfide phases ( $\text{Ni}_3\text{S}_2$  and  $\text{Ni}_3\text{S}_4$ ), and highly resistant to S poisoning.

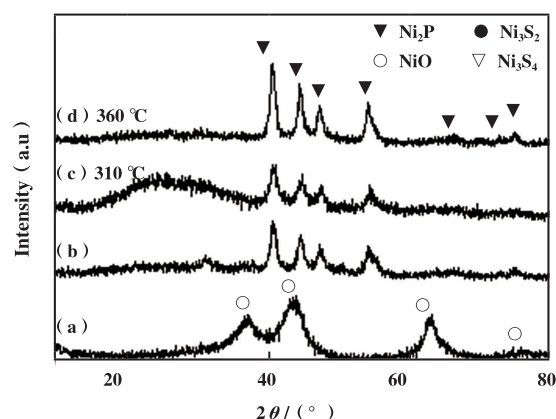


Fig.2 XRD patterns for the  $\text{Ni}/\text{Al}_2\text{O}_3$  calcined at 350 °C (a), followed by phosphidation of (a) at 320 °C for 36 h (b) and then sulfidation of (b) at 310~360 °C for 4 h (c and d), respectively

Table 2 displays the changes in the phases and crystalline sizes for the samples shown in Fig.2. The crystalline size of  $\text{Ni}_2\text{P}$  obtained by the direct phosphidation of  $\text{NiO}/\text{Al}_2\text{O}_3$  with  $\text{PPh}_3$  was about 7.0 nm. When the  $\text{Ni}_2\text{P}/\text{Al}_2\text{O}_3$  was treated by  $\text{CS}_2$  at 310 °C, both the  $\text{Ni}_2\text{P}$  phase and the crystalline size (6.7 nm) did not change. When it was treated at 360 °C, the  $\text{Ni}_2\text{P}$  phase still remained, but the crystalline size of  $\text{Ni}_2\text{P}$  increased to 9.5 nm, which was still significantly smaller than that formed by the phosphidation of  $\text{NiS}_x$  at 320 °C (13.3 nm), indicating the high stability of phase and crystalline size of  $\text{Ni}_2\text{P}$ .

Table 2 Phases and crystalline sizes in the catalysts prepared by different procedures

Samples in Fig.2	XRD phase	D /nm
a	NiO	3.0
b	$\text{Ni}_2\text{P}$	7.0
c	$\text{Ni}_2\text{P}$	6.7
d	$\text{Ni}_2\text{P}$	9.5

Notes: The crystalline sizes (D) were estimated by the Scherrer equation according to the full width at half maximum (FWHM) of the peaks at 43.2° (NiO) and 40.8° ( $\text{Ni}_2\text{P}$ ) respectively, in the XRD patterns.

Table 3 summarizes the information about the phases, crystalline sizes and compositions for the  $\text{NiS}_x/\text{Al}_2\text{O}_3$ ,  $\text{Ni}_2\text{P}/\text{Al}_2\text{O}_3$ ,  $\text{NiS}_x(\text{P})/\text{Al}_2\text{O}_3$  ( $\text{NiS}_x/\text{Al}_2\text{O}_3$  phosphided at 320 °C) and  $\text{Ni}_2\text{P}(\text{S})/\text{Al}_2\text{O}_3$  ( $\text{Ni}_2\text{P}/\text{Al}_2\text{O}_3$

sulfided at 310 °C). It is seen that only 3% sulfur remained in the  $\text{NiS}_x(\text{P})/\text{Al}_2\text{O}_3$ , i. e., most S in the  $\text{NiS}_x$  was replaced by P upon the phosphidation of  $\text{NiS}_x$  at 320 °C. In contrast, only 1.1% sulfur was incorporated into the  $\text{Ni}_2\text{P}(\text{S})/\text{Al}_2\text{O}_3$  when the  $\text{Ni}_2\text{P}/\text{Al}_2\text{O}_3$  was treated by  $\text{CS}_2$  at 310 °C, indicating that  $\text{Ni}_2\text{P}$  was highly resistant to

sulfur. The P/Ni atom ratios in the  $\text{NiS}_x(\text{P})/\text{Al}_2\text{O}_3$  and  $\text{Ni}_2\text{P}(\text{S})/\text{Al}_2\text{O}_3$  were similar (0.74), higher than the stoichiometric ratio of 0.5 for  $\text{Ni}_2\text{P}$ , probably due to the presence of some other phosphorus species in the catalysts<sup>[16]</sup>.

Table 3 Phases and crystalline sizes as well as chemical compositions analyzed by XRD and XRF for the catalysts prepared by different procedures

Catalyst	XRD Phase	D /nm	Ni/%	P/%	S/%	P/Ni (atom)	S/Ni (atom)
$\text{NiS}_x/\text{Al}_2\text{O}_3$	$\text{Ni}_3\text{S}_2$ , $\text{Ni}_3\text{S}_4$	5.8	—	—	—	—	—
$\text{Ni}_2\text{P}/\text{Al}_2\text{O}_3$	$\text{Ni}_2\text{P}$	7.0	—	—	—	—	—
$\text{NiS}_x(\text{P})/\text{Al}_2\text{O}_3$	$\text{Ni}_2\text{P}$	13.3	49.3	19.4	3.0	0.74	0.11
$\text{Ni}_2\text{P}(\text{S})/\text{Al}_2\text{O}_3$	$\text{Ni}_2\text{P}$	6.7	51.6	20.3	1.1	0.74	0.04

### 3.3 Hydrotreating activities of nickel sulfides and phosphides

The catalysts  $\text{NiS}_x/\text{Al}_2\text{O}_3$ ,  $\text{Ni}_2\text{P}/\text{Al}_2\text{O}_3$ ,  $\text{NiS}_x(\text{P})/\text{Al}_2\text{O}_3$  and  $\text{Ni}_2\text{P}(\text{S})/\text{Al}_2\text{O}_3$  were compared for the hydrotreating reactions. Fig.3 shows the XRD patterns of the used catalysts after the hydrotreating reactions. It is seen that  $\text{NiS}_x$  and  $\text{Ni}_2\text{P}$  phases in  $\text{NiS}_x/\text{Al}_2\text{O}_3$  (7.7 nm) and  $\text{Ni}_2\text{P}/\text{Al}_2\text{O}_3$  (8.0 nm) remained after the reactions (Fig.3 (a) and (c)), indicating that both  $\text{NiS}_x$  and  $\text{Ni}_2\text{P}$  phases were stable during the HDS reactions.

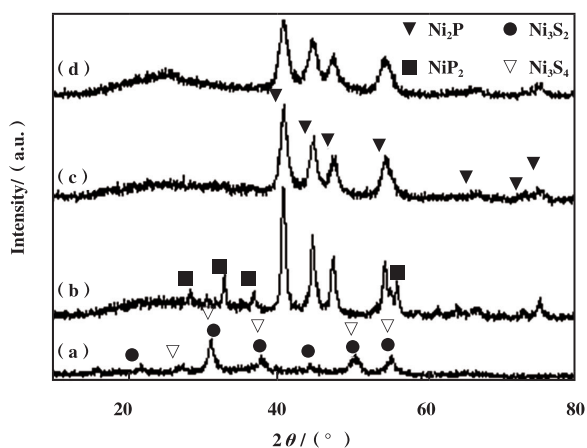


Fig.3 XRD patterns for the used catalysts after the HDS reactions:  $\text{NiS}_x/\text{Al}_2\text{O}_3$  (a),  $\text{NiS}_x(\text{P})/\text{Al}_2\text{O}_3$  (b),  $\text{Ni}_2\text{P}/\text{Al}_2\text{O}_3$  (c) and  $\text{Ni}_2\text{P}(\text{S})/\text{Al}_2\text{O}_3$  (d)

The diffraction peaks for  $\text{Ni}_2\text{P}$  in the  $\text{NiS}_x(\text{P})/\text{Al}_2\text{O}_3$

also remained with similar intensities ( $\sim 13.0$  nm) after the HDS reactions (Fig.3 (b)). However, some diffraction peaks for  $\text{NiP}_2$  (PDF 21-0590) were observed in the used catalyst after the HDS reaction. The reaction of  $\text{Ni}_2\text{P}$  with extra P in the catalyst during the HDS reaction might account for the formation of  $\text{NiP}_2$ .

The diffraction peaks for  $\text{Ni}_2\text{P}$  in the  $\text{Ni}_2\text{P}(\text{S})/\text{Al}_2\text{O}_3$  did not seem to change (7.0 nm) after the HDS reactions (Fig.3 (d)), indicating the high stability of  $\text{Ni}_2\text{P}$  in this catalyst.

Fig.4 (a) shows the activities of the  $\text{NiS}_x(\text{P})/\text{Al}_2\text{O}_3$ ,  $\text{Ni}_2\text{P}/\text{Al}_2\text{O}_3$ ,  $\text{NiS}_x(\text{P})/\text{Al}_2\text{O}_3$  and  $\text{Ni}_2\text{P}(\text{S})/\text{Al}_2\text{O}_3$  for the HDS of DBT. Apparently, the  $\text{Ni}_2\text{P}/\text{Al}_2\text{O}_3$  catalysts were significantly more active than the  $\text{NiS}_x/\text{Al}_2\text{O}_3$ . It is known that the  $\text{Ni}_2\text{P}$  was more active than sulfide catalysts for the hydrotreating reactions<sup>[14]</sup>. However, the comparisons were usually made between  $\text{Ni}_2\text{P}$  and the commercial Ni-Mo-S catalysts<sup>[14,20,31–33]</sup>. In the current work, the  $\text{Ni}_2\text{P}$  and  $\text{NiS}_x$  were prepared from the same precursor. In addition, the  $\text{NiS}_x/\text{Al}_2\text{O}_3$  (without Mo) prepared in this work showed the high activity for the HDS reaction. The conversion of DBT reached 75% at 360 °C. This must due to that the  $\text{NiS}_x/\text{Al}_2\text{O}_3$  catalysts were prepared from the highly dispersed  $\text{NiO}/\text{Al}_2\text{O}_3$  with small NiO particles ( $\sim 3$  nm).

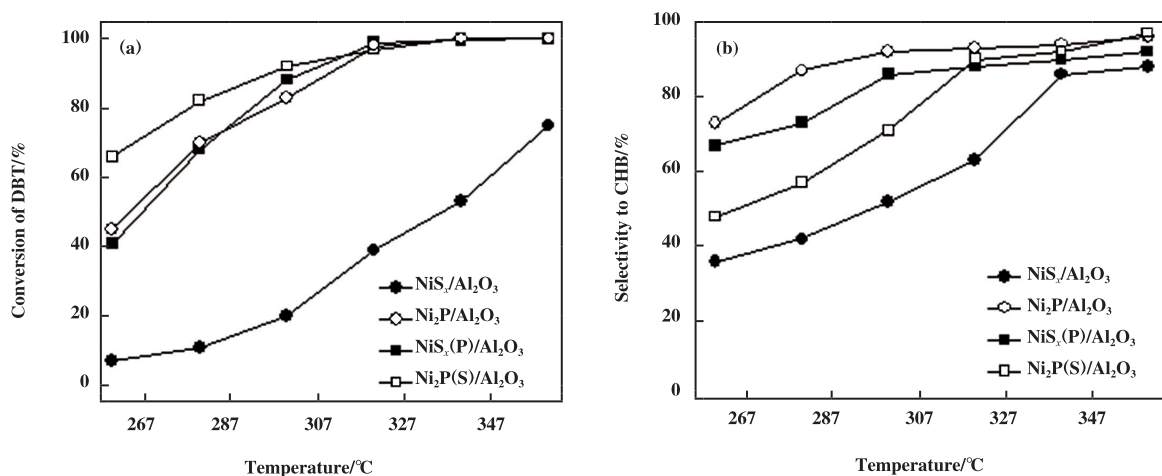


Fig.4 Conversion of DBT (a) and selectivity to cyclohexylbenzene (CHB)(b) over the catalysts

Reaction conditions: P=3.1 MPa, WHSV=2 h<sup>-1</sup> and H<sub>2</sub>/oil=1500 (v/v)

It is worth noting that the Ni<sub>2</sub>P (S)/Al<sub>2</sub>O<sub>3</sub> was more active than the Ni<sub>2</sub>P/Al<sub>2</sub>O<sub>3</sub> for the HDS of DBT. For example, at 260 °C, the conversion of DBT over the Ni<sub>2</sub>P (S)/Al<sub>2</sub>O<sub>3</sub> and Ni<sub>2</sub>P/Al<sub>2</sub>O<sub>3</sub> was about 66% and 45%, respectively. Some authors<sup>[19-22,34]</sup> proposed that the M-P-S (M=metal) species formed on the surfaces of transition metal phosphides during the HDS reactions might be the real active species. When the Ni<sub>2</sub>P/Al<sub>2</sub>O<sub>3</sub> was treated with CS<sub>2</sub>, the phase of Ni<sub>2</sub>P did not change, but some S (1.1%) was incorporated into the Ni<sub>2</sub>P (S)/Al<sub>2</sub>O<sub>3</sub> according to the XRF analysis. Thus, our current result agreed well with reported that surface Ni-P-S species must be more active than pure Ni<sub>2</sub>P for the HDS reactions.

The NiS<sub>x</sub> (P)/Al<sub>2</sub>O<sub>3</sub> contained 3% sulfur exhibited the similar activity to the Ni<sub>2</sub>P/Al<sub>2</sub>O<sub>3</sub> for the HDS reaction. However, the crystalline size of Ni<sub>2</sub>P in the NiS<sub>x</sub> (P)/Al<sub>2</sub>O<sub>3</sub> was significantly larger (13.3 nm) than that in the Ni<sub>2</sub>P/Al<sub>2</sub>O<sub>3</sub> (7.0 nm). Thus, the HDS activity of Ni<sub>2</sub>P in the NiS<sub>x</sub> (P)/Al<sub>2</sub>O<sub>3</sub> was significantly higher than that in the Ni<sub>2</sub>P/Al<sub>2</sub>O<sub>3</sub>, due to the presence of S.

The above results showed that the conversion of DBT at 360 °C followed the order of Ni<sub>2</sub>P (S)/Al<sub>2</sub>O<sub>3</sub> > NiS<sub>x</sub> (P)/Al<sub>2</sub>O<sub>3</sub> ~ Ni<sub>2</sub>P/Al<sub>2</sub>O<sub>3</sub> >> NiS<sub>x</sub>/Al<sub>2</sub>O<sub>3</sub>.

Fig.4 (b) shows the selectivities for the HDS of DBT over the catalysts at different temperatures. With the increase of temperature, the selectivity to cyclohexylbenzene (CHB) increased over all the

four catalysts. The high selectivity to CHB indicated that the HDS of DBT underwent mainly through the indirect desulfurization route (HYD) over the catalysts, where the desulfurization occurred after an aromatic ring in DBT was hydrogenated, rather than the direct desulfurization route (DDS) with the formation of biphenyl. It is also seen that the selectivity to CHB over the catalysts followed the order of Ni<sub>2</sub>P/Al<sub>2</sub>O<sub>3</sub> > NiS<sub>x</sub> (P)/Al<sub>2</sub>O<sub>3</sub> > Ni<sub>2</sub>P (S)/Al<sub>2</sub>O<sub>3</sub> > NiS<sub>x</sub>/Al<sub>2</sub>O<sub>3</sub>, indicating that the presence of sulfur might be unfavorable to the HYD route over Ni<sub>2</sub>P for the HDS of DBT.

Fig.5 shows the results for the conversion of quinoline and selectivity to propyl-cyclohexane (PCH) over the catalysts at different temperatures. The conversion of quinoline over all the catalysts reached 100% at 260~360 °C, indicating the high HDN activity of these catalysts. Although the selectivity to PCH increased with temperature over the catalysts, the catalysts exhibited different selectivities to PCH (especially at low temperatures). For example, the selectivity to PCH at 260 °C over the NiS<sub>x</sub>/Al<sub>2</sub>O<sub>3</sub>, Ni<sub>2</sub>P/Al<sub>2</sub>O<sub>3</sub>, Ni<sub>2</sub>P (S)/Al<sub>2</sub>O<sub>3</sub> and NiS<sub>x</sub> (P)/Al<sub>2</sub>O<sub>3</sub> were about 30%, 90%, 80% and 88%, respectively, indicating that Ni<sub>2</sub>P was much more active than NiS<sub>x</sub> for the hydrogenation of aromatic ring in quinoline.

Fig.6 (a) shows the conversions of tetralin over the catalysts. It is seen again that the Ni<sub>2</sub>P (S)/Al<sub>2</sub>O<sub>3</sub> catalyst exhibited much higher activities than the

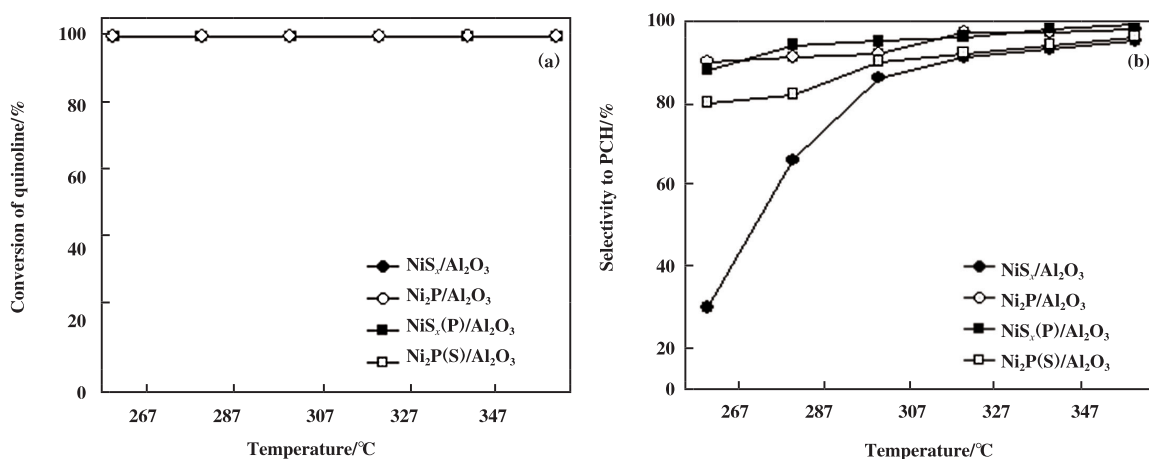


Fig.5 Conversion of quinoline (a) and selectivity to propyl-cyclohexane (PCH) (b) over the catalysts

Reaction conditions:  $P=3.1$  MPa,  $WHSV=2$  h<sup>-1</sup> and  $H_2/oil=1500$  (v/v)

$Ni_2P/Al_2O_3$  and  $NiS_x/Al_2O_3$  catalysts. For example, the conversion of tetralin at 360 °C was only 0.6% over the  $NiS_x/Al_2O_3$ , while that was 5.7%, 9.2% and 13.8%

over the  $NiS_x(P)/Al_2O_3$ ,  $Ni_2P/Al_2O_3$  and  $Ni_2P(S)/Al_2O_3$ , respectively, in consistence with the results for the HDS of DBT.

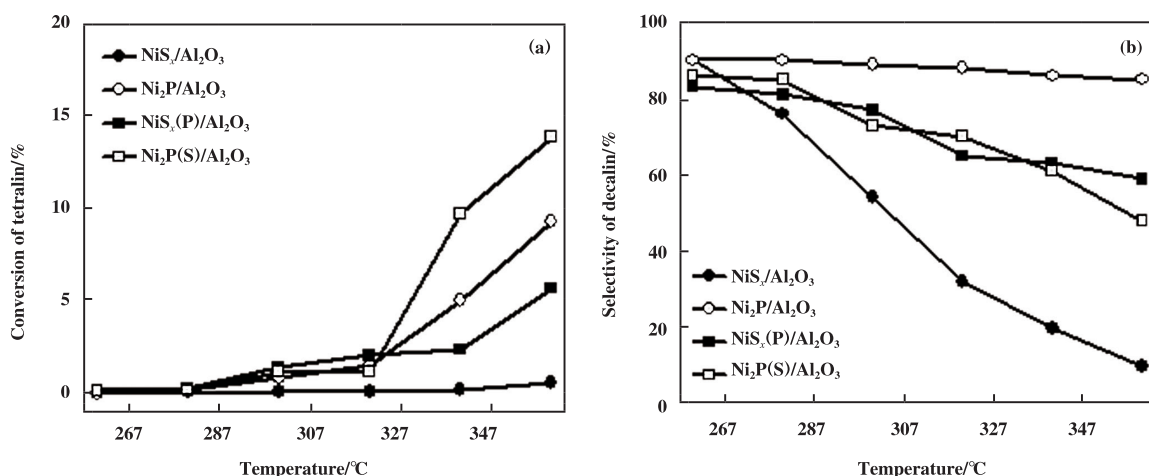


Fig.6 Conversion of tetralin (a) and the selectivity to decalin (b) over the catalysts

Reaction conditions:  $P=3.1$  MPa,  $WHSV=2$  h<sup>-1</sup> and  $H_2/oil=1500$  (v/v)

Tetralin might be hydrogenated to decalin or dehydrogenated to naphthalene during the hydrotreating reactions. Fig.6 (b) shows the selectivity to decalin over the catalysts. Apparently,  $Ni_2P$  exhibited much higher selectivity to decalin than  $NiS_x$ , and the  $Ni_2P$  catalysts containing a small amount of S showed the moderate selectivities, indicating again that the presence of S was unfavorable to the hydrogenation of aromatic rings.

## 4 Conclusions

A highly loaded and dispersed 80%  $Ni/Al_2O_3$

catalyst was prepared and calcined at 350 °C to obtain a  $NiO/Al_2O_3$  sample with small  $NiO$  particles ( $\sim 3$  nm). Then the  $NiO/Al_2O_3$  was sulfided by  $CS_2$  at 310 °C to  $NiS_x/Al_2O_3$  ( $Ni_3S_2$  and  $Ni_3S_4$ ) or phosphided by  $PPh_3$  at 320 °C to  $Ni_2P/Al_2O_3$ .

When the  $NiS_x/Al_2O_3$  was phosphided with  $PPh_3$  at 320 °C,  $NiS_x$  was converted into  $Ni_2P$  (13.3 nm) ( $NiS_x(P)/Al_2O_3$ ), which was as active as the directly phosphided  $Ni_2P/Al_2O_3$  (7.0 nm), indicating that the Ni-P-S species must be more active than the Ni-P species for the HDS of DBT, consistent with the results



reported<sup>[20-21]</sup>.

When the Ni<sub>2</sub>P/Al<sub>2</sub>O<sub>3</sub> was treated with CS<sub>2</sub> at 310~360 °C, the Ni<sub>2</sub>P phase did not change, indicating that Ni<sub>2</sub>P was much more stable than NiS<sub>x</sub> (Ni<sub>3</sub>S<sub>2</sub> and Ni<sub>3</sub>S<sub>4</sub>). Moreover, the Ni<sub>2</sub>P (S)/Al<sub>2</sub>O<sub>3</sub> (6.7 nm) treated with CS<sub>2</sub> at 310 °C was more active than the directly phosphided Ni<sub>2</sub>P/Al<sub>2</sub>O<sub>3</sub> (7.0 nm), indicating again that the Ni-P-S species must be more active than the Ni-P species for the HDS of DBT.

**Acknowledgments:** Financial supports from the NSFC (21773108), NSFC-DFG (21761132006) and fundamental research funds for central universities are acknowledged.

#### 参考文献:

- [1] Zhang Y, Wang Y, Jiang H, *et al.* Multifunctional nickel sulfide nanosheet arrays for solar-intensified oxygen evolution reaction[J]. *Small*, 2020, **16**: 2002550.
- [2] Muthu N S, Gopalan M. Mesoporous nickel sulphide nanostructures for enhanced supercapacitor performance[J]. *Appl Surf Sci*, 2019, **480**: 186–198.
- [3] Zhao H, Zhang H Z, Cui G W, *et al.* A photochemical synthesis route to typical transition metal sulfides as highly efficient cocatalyst for hydrogen evolution: from the case of NiS/g-C<sub>3</sub>N<sub>4</sub> [J]. *Appl Catal B-Environ*, 2018, **225**: 284–290.
- [4] You B, Sun Y. Hierarchically porous nickel sulfide multifunctional superstructures[J]. *Adv Energy Mater*, 2016, **6**: 1502333.
- [5] Peters A W, Li Z, Farha O K, *et al.* Toward inexpensive photocatalytic hydrogen evolution: a nickel sulfide catalyst supported on a high-stability metal-organic framework[J]. *ACS Appl Mater Interfaces*, 2016, **8**(32): 20675–20681.
- [6] Zhao Yuan-yuan(赵媛媛), Duan Zhen-wei(段振伟), Qi Sheng-jie(祁胜杰), *et al.* Synthesis and performance of hydro-desulfurization (HDS) catalyst Ni/Al<sub>2</sub>O<sub>3</sub> with Ni-Al hydrotalcite-like compounds as precursors(Ni-Al类水滑石的制备及其Ni/Al<sub>2</sub>O<sub>3</sub> 加氢脱硫研究) [J]. *J Mol Catal (China)*(分子催化), 2014, **28**(5): 418–426.
- [7] Welters W J J, Vorbeck G, Zangbergen H W, *et al.* HDS activity and characterization of zeolite-supported nickel sulfide catalysts[J]. *J Catal*, 1994, **150**(1): 155–169.
- [8] Cid R, Atanasova P, López-Cordero R, *et al.* Gas oil hydrodesulfurization and pyridine hydrodenitrogenation over NaY-supported nickel sulfide catalysts: Effect of Ni loading and preparation method[J]. *J Catal*, 1999, **182**(2): 328–338.
- [9] Ramos R R, Bolivar C, Castillo J, *et al.* Ultrasound assisted synthesis of nanometric Ni, Co, NiMo and CoMo HDS catalysts[J]. *Catal Today*, 2008, **133/135**: 277–281.
- [10] Mondal D, Villemure G, Li G C, *et al.* Synthesis, characterization and evaluation of unsupported porous NiS<sub>2</sub> sub-micrometer spheres as a potential hydrodesulfurization catalyst[J]. *Appl Catal A-Gen*, 2013, **450**: 230–236.
- [11] Ho T C. Hydrodenitrogenation catalysis[J]. *Catal Rev-Sci Eng*, 1988, **30**(1): 117–160.
- [12] Prins R, De Beer V H J, Somorjai G A. Structure and function of the catalyst and the promoter in Co-Mo hydrodesulfurization catalysts[J]. *Catal Rev-Sci Eng*, 1989, **31**(1/2): 1–41.
- [13] Lai W K, Chen Z, Zhu J P, *et al.* A NiMoS flower-like structure with self-assembled nanosheets as high-performance hydrodesulfurization catalysts[J]. *Nanoscale*, 2016, **8**(6): 3823–3833.
- [14] Oyama S T, Gott T, Zhao H, *et al.* Transition metal phosphide hydroprocessing catalysts: A review[J]. *Catal Today*, 2009, **143**(1/2): 94–107.
- [15] Zhao Y, Xue M, Cao M, *et al.* A highly loaded and dispersed Ni<sub>2</sub>P/SiO<sub>2</sub> catalyst for the hydrotreating reactions[J]. *Appl Catal B-Environ*, 2011, **104**(3/4): 229–233.
- [16] Wang J E, Chen H, Fu Y C, *et al.* Highly active Ni<sub>2</sub>P/SiO<sub>2</sub> catalysts phosphorized by triphenylphosphine in liquid phase for the hydrotreating reactions[J]. *Appl Catal B-Environ*, 2014, **160/161**: 344–355.
- [17] Phimsen S, Kiatkittipong W, Yamada H, *et al.* Nickel sulfide, nickel phosphide and nickel carbide catalysts for bio-hydrotreated fuel production[J]. *Energy Convers Manage*, 2017, **151**: 324–333.
- [18] Stinner C, Prins R, Weber T. Binary and ternary transition-metal phosphides as HDN catalysts[J]. *J Catal*, 2001, **202**(1): 187–194.
- [19] Oyama S T, Wang X, Lee Y K, *et al.* Effect of phosphorus content in nickel phosphide catalysts studied by XAFS and other techniques[J]. *J Catal*, 2002, **210**(1): 207–217.
- [20] Oyama S T, Wang X, Lee Y K, *et al.* Active phase of Ni<sub>2</sub>P/SiO<sub>2</sub> in hydroprocessing reactions[J]. *J Catal*, 2004, **221**(2): 263–273.

- [ 21 ] Duan X P, Teng Y, Wang A J, *et al.* Role of sulfur in hydrotreating catalysis over nickel phosphide[ J ]. *J Catal*, 2009, **261**(2): 232–240.
- [ 22 ] Song L M, Zhang S J, Ma Q Y. Synthesis of an iron phosphide catalyst based on sulfides and hydrodesulfurization property[ J ]. *Chem Eng J*, 2015, **281**: 281–285.
- [ 23 ] Nelson A E, Sun M, Junaid A S M. On the structure and composition of the phosphosulfide overlayer on Ni<sub>2</sub>P at hydrotreating conditions[ J ]. *J Catal*, 2006, **241**(1): 180–188.
- [ 24 ] Wang J E, Fu Y C, Chen H, *et al.* Effect of supports on the supported Ni<sub>2</sub>P catalysts prepared by the phosphidation using triphenylphosphine in liquid phase[ J ]. *Chem Eng J*, 2015, **275**: 89–101.
- [ 25 ] Wang J E, Yuan Y M, Shuai A, *et al.* Effect of ZrO<sub>2</sub> in Ni<sub>2</sub>P/ZrO<sub>2</sub>-Al<sub>2</sub>O<sub>3</sub> catalysts on hydrotreating reactions[ J ]. *RSC Adv*, 2015, **5**: 74312–74319.
- [ 26 ] Wang J E, Li S Z, Xu J, *et al.* Effect of loading on the Ni<sub>2</sub>P/Al<sub>2</sub>O<sub>3</sub> catalysts for the hydrotreating reactions[ J ]. *J Energy Chem*, 2015, **24**(4): 441–447.
- [ 27 ] Wang J E, Wang X G, Yuan Y M, *et al.* Optimization of MgO/Al<sub>2</sub>O<sub>3</sub> ratio for the maximization of active site densities in the Ni<sub>2</sub>P/MgAlO catalysts for the hydrotreating reactions[ J ]. *J Energy Chem*, 2016, **25**(4): 571–576.
- [ 28 ] Yuan Y M, Pei H, Chen H, *et al.* Preparation of Fe<sub>2</sub>P and FeP catalysts for the hydrotreating reactions[ J ]. *Catal Commun*, 2017, **100**: 202–205.
- [ 29 ] Yuan Y M, Zhang J Y, Chen H, *et al.* Preparation of Fe<sub>2</sub>P/Al<sub>2</sub>O<sub>3</sub> and FeP/Al<sub>2</sub>O<sub>3</sub> catalysts for the hydrotreating reactions[ J ]. *J Energy Chem*, 2019, **29**: 116–121.
- [ 30 ] Shi G J, Shen J Y. Skeletal isomerization of 1-hexene over sulfided Co/Co-MCM-41 catalysts[ J ]. *Energy Fuels*, 2009, **23**(1): 320–326.
- [ 31 ] Oyama S T. Novel catalysts for advanced hydroprocessing: Transition metal phosphides[ J ]. *J Catal*, 2003, **216**(1/2): 343–352.
- [ 32 ] Wang X, Clark P, Oyama S T. Synthesis, characterization, and hydrotreating activity of several iron group transition metal phosphides[ J ]. *J Catal*, 2002, **208**(2): 321–331.
- [ 33 ] Lee Y K, Oyama S T. Sulfur resistant nature of Ni<sub>2</sub>P catalyst in deep hydrodesulfurization[ J ]. *Appl Catal A-Gen*, 2017, **548**: 103–113.
- [ 34 ] Zhou X R, Li X, Prins R, *et al.* Desulfurization of 2-phenylcyclohexanethiol over transition-metal phosphides[ J ]. *J Catal*, 2020, **383**: 331–342.

## Stability and Activity of Ni<sub>2</sub>P and NiS<sub>x</sub> for the Hydrotreating Reactions

YUAN Ya-mei, CHEN Hui\*, ZHAO Dan-yang, WU Chi, GENG Jiao\*, SHEN Jian-yi\*

( Laboratory of Mesoscopic Chemistry, School of Chemistry and Chemical Engineering,  
Nanjing University, Nanjing 210023, China )

**Abstract:** A highly dispersed 80% Ni/Al<sub>2</sub>O<sub>3</sub> catalyst was prepared by the co-precipitation method, which was calcined in air at 350 °C to obtain a highly dispersed NiO/Al<sub>2</sub>O<sub>3</sub> with NiO particles of about 3 nm. The NiO/Al<sub>2</sub>O<sub>3</sub> was then sulfided with CS<sub>2</sub> at 310 °C to nickel sulfides ( Ni<sub>3</sub>S<sub>2</sub> and Ni<sub>3</sub>S<sub>4</sub> of about 5.8 nm ), or phosphided with PPh<sub>3</sub> at 320 °C to Ni<sub>2</sub>P ( 7.0 nm ). The NiS<sub>x</sub> phases were completely converted into Ni<sub>2</sub>P ( 13.3 nm ) when phosphided with PPh<sub>3</sub> at 320 °C, which was as active as the directly phosphided Ni<sub>2</sub>P ( 7.0 nm ). In contrast, the phase and crystalline size of Ni<sub>2</sub>P did not change when treated with CS<sub>2</sub> even at 360 °C, indicating that the Ni<sub>2</sub>P was much more stable than the NiS<sub>x</sub> ( Ni<sub>3</sub>S<sub>2</sub> and Ni<sub>3</sub>S<sub>4</sub> ). Moreover, the Ni<sub>2</sub>P/Al<sub>2</sub>O<sub>3</sub> treated with CS<sub>2</sub> at 310 °C was more active than the directly phosphided Ni<sub>2</sub>P for the hydrodesulfurization ( HDS ) reaction, indicating that the incorporation of S into Ni<sub>2</sub>P might generate some Ni-P-S species that were more active than the Ni-P surface species for the HDS reactions.

**Key words:** Ni<sub>2</sub>P/Al<sub>2</sub>O<sub>3</sub> catalyst; NiS<sub>x</sub>/Al<sub>2</sub>O<sub>3</sub> catalyst; liquid phase phosphidation by PPh<sub>3</sub>; liquid phase sulfidation by CS<sub>2</sub>; phase stability; hydrotreating reaction